Markstein Numbers of Negatively-Stretched Premixed Flames - Microgravity Measurements and Computations

Alfonso F. Ibarreta[1], James F. Driscoll[1], and Douglas A. Feikema[2]

[1]University of Michigan, Department of Aerospace Engineering, Ann Arbor, MI 48109

[2]NASA Glenn Research Center, Microgravity Science Division, Cleveland, OH 44135

Abstract

The effect of flame stretch, composed of strain and curvature, plays a major role in the propagation of turbulent premixed flames. Although all forms of stretch (positive and negative) are present in turbulent conditions, little research has been focused on the stretch due to curvature. The present study quantifies the Markstein number (which characterizes the sensitivity of the flame propagation speed to the imposed stretch rate) for an inwardly-propagating flame (IPF). This flame is of interest because it is negatively-stretched, and is subjected to curvature effects alone, without the competing effects of strain. In an extension of our previous work, microgravity experiments were run using a vortex-flame interaction to create a pocket of reactants surrounded by an IPF. Computations using the RUN-1DL code of Rogg were also performed in order to explain the measurements.

It was found that the Markstein number of an inwardly-propagating flame, for both the microgravity experiment and the computations, is significantly larger than that of an outwardly-propagating flame. Further insight was gained by running the computations for the simplified (hypothetical) cases of one-step chemistry, unity Lewis number, and negligible heat release. Results provide additional evidence that the Markstein numbers associated with strain and curvature have different values.

Submitted to the Twenty-Ninth Symposium (International) on Combustion

ADDRESS Alfonso F. Ibarreta
University of Michigan, Dept. of Aerospace Engineering
1320 Beal Avenue (FXB), Ann Arbor, MI 48109, USA
email: aibarret@engin.umich.edu fax: (734)763-0578

COLLOQUIUM LAMINAR FLAMES: (#4)
Laminar-Premixed
Laminar Dynamics

Words in Manuscript: (counted using Word)	3251
Equations: 21 words/equation X 5	105
Figures 1-7: 200 words/figure X 7	1400
Figure 8 : 400 words/figure X 1	400
References: 7 words/line X 33	231
Total Words:	5387

Choice of Presentation: Oral

INTRODUCTION

Because turbulence exerts both curvature and strain on a premixed flame, there have been numerous studies of how flames react to both of these conditions [1–11]. However, most of these studies have focused on strained flames, such as the counterflow flame case [1] or flames with positive strain and curvature such as the spherical outwardly-propagating flame (OPF) [2–5]. The present work instead focuses on one type of negatively-stretched flame, namely the inwardly-propagating flame (IPF). The IPF has the desirable property that the stretch rate (normally composed of both strain and curvature) consists of curvature effects alone. The complicating effects of strain are not present, since the gas ahead of the IPF is at rest. Ideally, it would be useful to quantify the Markstein number, which represents the sensitivity of the propagation speed to the imposed stretch rate, for four conditions: positive strain alone (the counterflow case), positive curvature alone, negative strain alone, and negative curvature alone (which is the IPF condition). Simple theory predicts that the Markstein number, *Ma*, will be the same for all four of these conditions (at the same fuel-air equivalence ratio Φ). However, results of Bradley et al. [5], Echekki and Mungal [6], Poinsot et al. [7], Durox et al. [8], and Ibarreta and Driscoll [9] indicate that there may be different values of Ma associated with each of these four cases.

The present work builds upon a previous experimental study [9] conducted at 1-g, in which it was shown that Ma for an IPF is two to three times larger than that of a corresponding OPF. In the present work the experiment is operated in microgravity, which removes the complications of buoyancy and flame-produced vorticity [12, 13], and a full set of numerical computations are conducted, using the RUN-1DL code of Rogg [14, 15] with complex chemistry, to better explain the experimental results. Computed values of Ma are reported for both the OPF and the IPF cases, and are compared to the measurements. An advantage of the experiment is that a nearly spherical IPF is formed in the latter stages of the burnup of a pocket of reactants. This spherical geometry allows for accurate measurement of flame speed since the reactants are essentially at rest. Previous measurements of negatively-stretched flames have been reported for more complicated geometries [6–8, 10, 11, 16].

The Markstein number (Ma) that was measured relates the stretched burning velocity, S_u, to its un-

stretched value, S_u^o, through the following relation:

$$S_u / S_u^o = 1 - Ma\, Ka \qquad (1)$$

This equation is based on the original analysis of Markstein [12] and the Wenzel definition of Karlovitz number:

$$Ka = K / \left[(S_u)^2 / D_u \right] \qquad (2)$$

Where K is the stretch rate; Kwon et al. [2] have suggested the normalization factor that appears in Eq. 2, which depends on the local burning velocity of the stretched flame (S_u). D_u is the binary diffusivity of the fuel into nitrogen. The burning velocity is defined as the speed of flame propagation relative to the unburned reactants. The stretch rate [17] equals $\left| A^{-1} dA/dt \right|$, where A is an infinitesimal area of flame surface. Note that other researchers have chosen to nondimensionalize the stretch rate using the unstretched velocity, S_u^o, rather than S_u. This leads to a relation that is slightly different from Eq. 1, for which the right side is $(1 - Ma\, Ka)$. Both relations yield exactly the same values of Ma in the limit as Ka approaches zero. However, experiments show that Eq. 1 provides a good fit to experimental data (as shown below) for moderate values of Ka, and thus provides an accurate method to determine values of Ma.

MICROGRAVITY EXPERIMENT

The experimental setup is similar to a previous 1-g experiment [9] that was modified to be operated at microgravity conditions in the NASA Glenn 2.2 Second Drop Tower. A premixed propane-air flame, at an equivalence ratio (Φ) of 0.54, is interacted with a vortex propagating in the opposite direction, causing the flame to wrap around the vortex. The distorted flame surface eventually pinches off from the main surface, creating a pocket of reactants surrounded by an IPF. Long after the vortex has been convected away and has decayed, the IPF burns from an initial diameter of approximately 10 mm to a final observed diameter of less than 1 mm. The combustion chamber is 11.4 cm by 11.4 cm by 23.5 cm and has a loudspeaker at one end to force gas through a 2.54 cm orifice, creating the toroidal vortex. In a series of events programmed into a Tattletale controller, an electrical connection is broken which signals the beginning of the drop; after a 500 ms wait time, exhaust ports are opened to prevent pressure buildup and the flame is ignited using a

spark. After 200 ms the speaker is pulsed and the pocket formation occurs 300 - 400 ms later. Final pocket collapse occurs in another 100 ms, so the entire process takes less than 1 second.

Flame speeds were measured by recording shadowgraph images of the pockets at 500 frames/sec and using a Kodak RO digital camera. Figure 1 shows the digitized image of the flame boundary at four different times. Since the actual flame is not perfectly spherical, the boundary at each frame was fitted with a polynomial and then divided into 400 flame segments to determine the local normal vector and the burning velocity (S_u), which is: $S_u = \Delta X_n/\Delta t$. The distance from one segment of the flame front to the flamefront in the next image is ΔX_n, as measured along the normal direction, and Δt is the time between images. Candel and Poinsot [18] have shown that the stretch rate (K) is $-\vec{n}\cdot(\vec{n}\cdot\nabla)\vec{u} + \nabla\cdot\vec{u} + S_u/R_c$. For the IPF the velocity of the gas ($\vec{u}$) inside the pocket is zero due to symmetry, so the stretch rate of an IPF is:

$$K = S_u/R_c, \tag{3}$$

The radius of curvature, R_c, was calculated for each segment from its in-plane and out-of-plane components, assuming that the pocket is symmetrical about the vertical axis. The measured Markstein number was determined for the IPF by combining Eqs. 1-3 and solving for S_u, which yields:

$$S_u/S_u^o = 1 - Ma\ \delta_D^o/R_c \tag{4}$$

The unstretched flame thickness δ_D^o is defined as D_u/S_u^o. This gives us a simple relation between the burning velocity and the flame curvature (normalized by δ_D^o). Note that R_c is a negative number for the IPF geometry considered.

NUMERICAL SIMULATIONS

To explain the experimental findings, numerical simulations of both inwardly and outwardly propagating spherical flames (with complex chemistry) were generated using the RUN-1DL code of Rogg [14, 15]. This computer code solves the time-dependant conservation equations in spherical coordinates. An adaptive grid tracks the flame front as it moves in time. Experimental conditions were matched by considering a lean propane-air flame with initial conditions of 300 K and 1 atm. Symmetric boundary conditions are enforced both at the origin and at the edge of the domain, so that the gradients of temperature and of species mass

fractions at the boundaries are set to equal zero. The propane-air detailed chemical mechanism of Djavdan et al. [19] was used which includes 29 species and 61 reactions and predicts an unstretched burning velocity that agrees with experimental data of Egolfopoulos et al. [20] to within 20%. To examine if the same trends in the computed Markstein numbers are valid for other hydrocarbon fuel, methane-air cases were also computed using the detailed chemistry of Smooke et al. [21] that includes 16 species and 46 reactions and predicts an unstretched burning velocity that agrees with experimental data [22] to within 10%. In addition, the role of intermediate species was investigated by removing intermediates from the calculation entirely; values of Ma were calculated for simple-one step methane-air chemistry and were compared to the complex chemistry results. For the one-step chemistry, an activation energy of 50 $kcal/mol$ and an Arrhenius pre-exponential factor of $4.4 \cdot 10^{-15}$ yield a stoichiometric unstretched burning velocity that agrees with experiments [22] to within 10%.

The computed flame boundary was defined as the radial location of maximum temperature gradient, since this is comparable to the boundary defined by the shadowgraph images obtained in the experiment. For the IPF computations, the stretch rate was determined using Eq. 3 and the local burning velocity was determined using:

$$S_u = d\,r_u\,/dt \tag{5}$$

since the gas velocity ahead of the IPF is zero; r_u is defined as the radial position of the flame surface. The computed Markstein numbers for the IPF were determined by combining Eqs. 4 and 5.

For the computed outwardly-propagating flame, the gas velocity ahead of the flame is not zero, so Eqs. 3 - 5 are not applicable. Instead, the stretch rate and the local burning velocity for the spherical OPF can be shown [2] to be $[(2/\,r_u)\cdot d\,r_u\,/dt]$ and $[(\rho_b/\rho_u)\cdot d\,r_u\,/dt]$, respectively. Once K and S_u are computed in this manner, the Markstein number of the OPF is found using Eq. 1 and 2.

Several researchers have published corrections for the Markstein number of the OPF related to accumulation and traverse fluxes along the flamefront due to the finite flame thickness [1, 5, 23, 24]. There is disagreement, however, between each of the corrections which depend heavily on the definition of the flame thickness and therefore add ambiguity to the results. It was decided not to apply the corrections in the current work, so that the flame is assumed to be infinitely thin with respect to the radius of curvature. It is

important to note that none of the corrections apply to the IPF configuration.

RESULTS

Figure 2 shows some results of the microgravity IPF experiment, for which the propane-air equivalence ratio was 0.54. The slope of the curve in Fig. 2 is $(-Ma)$, in accordance with Eq. 4. Figure 2 was obtained by compiling about 2000 data points from one drop; the flame boundaries were divided into segments and the local curvature and burning velocity were calculated as described earlier. The data were then grouped according to curvature $(1/R_c)$ and plotted. Each solid symbol represents the mean burning velocity for the points in each of the curvature groups. The error bars represent the range from +1 to -1 standard deviations (σ) from the mean of the group. Note that the uncertainty in determining the mean value (i.e. the solid symbol) is much less than the height of the error bars drawn. Figure 2 shows that, despite the large amount of scatter associated with this difficult experiment, there appears to be a linear relation between the variables plotted; therefore Eq. 4 is valid. The slope of the data in Fig. 2 yields a Markstein number of 12.1.

Figure 3 shows some numerical results obtained using the RUN-1DL for both OPF and IPF cases, with complex propane-air chemistry at $\Phi = 0.6$. The slope of the curve for the IPF (i.e. negative Karlovitz numbers) yields a Markstein number of 11.5, which is within the range of values that were measured in the microgravity experiment. The difference in slopes seen in Figure 3 also indicate that the Markstein number of the computed IPF is larger than that of the corresponding OPF.

Comparisons are made in Fig. 4 between the Markstein numbers obtained in the experiment, the computed IPF, and the computed OPF cases. There is satisfactory agreement between the experimental IPF values (solid diamonds) and the computed IPF values (solid triangles). Also shown are the results of Sun et al. [1], represented by the solid circles. Sun et al. also performed IPF computations for complex propane-air chemistry, and their results lie within 20% of the present values. The OPF results of the present work are shown as open triangles. Also shown are OPF results from experiments [3, 4, 25, 26] and from computations. It can be concluded from Fig. 4 that in all cases the Markstein numbers associated with the IPF are 2-3 times larger than those for the OPF.

The numerical results are useful in that they show how positive and negative stretch affect the profiles

of species concentrations and temperature across the flame. Two examples are given by the IPF profiles shown in Fig. 5 and the OPF profiles seen in Fig. 6. [illegible] [illegible] by the negative stretch that is exerted (as compared to the unstretched flame). This trend is expected: the value of Ma is positive and the negative stretch exerted causes an increase in the burning velocity, as given by Eq. 1. A similar and expected increase in the OH and H radical concentrations is also observed.

In Fig. 6 the reverse trend occurs, as expected. As positive stretch is exerted, the temperatures within the stretched case (solid line) now lie below those of the unstretched case (dotted line). This decrease in flame temperature is tied to a decrease of radical concentrations such as OH and H, and also corresponds to a decrease in burning velocity.

An interesting difference between the IPF and OPF is that there is a buildup of hydrogen molecules ahead of the IPF (see Fig. 5), but no such buildup occurs for the OPF. This effect is due to the zero-gradient boundary condition at the origin, which allows the H_2 diffusing upstream of the IPF flame to accumulate. This mimics the flame-flame interaction that would occur in the IPF during the very late stages of pocket burnup. The influence of this effect was quantified by changing the boundary condition and setting the mole fractions constant at $r = 0$. No significant change in the Markstein number was observed, thus flame-flame interaction was assumed to be trivial for the range of stretch values we are interested in.

To determine if the above results are unique to propane-air flames, or are also observed for other hydrocarbon fuels, the computations were repeated for methane-air flames with complex chemistry. Figure 7 shows that the methane-air flames are similar to propane-air flames in that the values of Ma for the IPF (solid triangles) are more than 2 - 3 times larger than for the OPF. The values of Ma computed for the OPF cases are in agreement with the OPF values measured by Tseng et al. [3, 25], which are represented by the open circles in Fig. 7.

Since the computational results agree with the experimental finding that values of Ma are larger for the IPF than for the OPF case, it was decided to determine if radicals and intermediates cause this difference. Therefore radicals and intermediates were removed by running the RUN-1DL code using one-step chemistry. The one-step chemistry results are compared to the complex chemistry results in Fig. 7. For this comparison,

methane-air mixtures were considered, since a number of researchers have proposed global or quasi-global reaction schemes for this type of fuel [27]. Figure 8a shows the [illegible] this computation. Figure 7 shows that one-step chemistry does predict values of Markstein number (the solid diamond symbols) that are in reasonable agreement with the complex chemistry results (the solid triangles). The one-step chemistry results also predict that Ma for the IPF case is larger than that for the OPF case. It is concluded that the presence of radicals and intermediate species is not the primary factor that causes the difference in Markstein number of the IPF and OPF cases.

Another computation was performed to determine the role, if any, of the Lewis number of the deficient reactant. The Lewis number (Le) is defined for each species as the ratio of the thermal diffusivity to the mass diffusivity of the species. The RUN-1DL code was run for a simple one-step methane-air chemistry using values found by Coffee [28]; the Lewis number of each species, except for the fuel, was set to one. The fuel Lewis number (Le_F) was varied to observe its effects on the Markstein number. Figure 8a shows that for these simplified conditions, the Markstein number is, as expected, directly related to the Lewis number of the deficient reactant. There is still, however, an unexplained difference in the IPF and OPF Markstein numbers. This difference increases for larger Lewis numbers.

Finally, the role that thermal expansion plays in determining the Markstein number was investigated. For an OPF, thermal expansion caused by heat release increases the velocity of the reactants ahead of the flame and creates a strain field, since the expanding flame acts as a piston. To study the flame without this complicated effect, the heat release rates for both IPF and OPF cases were set to be nearly zero. RUN-1DL computations were obtained with single-step chemistry and for sufficiently small enthalpy of combustion such that the temperature rise across the flame was only 10%. Other constants, such as activation energy, were adjusted to yield an unstretched burning velocity similar to that of a methane-air mixture at the same equivalence ratio (0.66). Results for this cool flame simulation are seen in Fig. 8b. These results show that Markstein number is identical for both the IPF and OPF cases over a wide range of conditions if heat release is absent. Therefore the differences in Markstein number between the OPF and IPF cases can be attributed to different values of Markstein number associated with the strain field and the curvature effects. Other studies which have investigated these differences have been conducted by Poinsot et al. [7] and Bradley et

al. [5].

UNCERTAINTY ANALYSIS

Experimental uncertainties for this study have been documented in Ref. 9. The computational uncertainties were determined by varying the number of grid points, the initial conditions, and the domain size. The number of radial grid points was chosen to be between 100 and 140; a sample calculation was performed with half the normal number of grid points and the resulting value of Ma changed by less than 5%. To specify the initial conditions, the entire domain is initially composed of only reactants, and a Gaussian-shaped temperature profile is imposed at outermost radial location of the domain, causing the mixture to ignite and the flame to burn inward. The excess enthalpy associated with this ignition source rapidly diffuses radially out of the domain. To insure that the results are independent of the initial temperature profile chosen, the value of the maximum initial temperature was raised from 1700 K to 2400 K. For both of these values the flame profiles quickly adjusted to become identical, and the resulting values of *Ma* differed by less than 1%. The domain size ideally would be infinite, but it was found that values of Ma varied by less than 3% if the domain size was varied from 5 cm to 9 cm, so values in this range were used.

CONCLUSIONS

1. Markstein numbers of a inwardly-propagating flame (IPF) were measured in microgravity using a unique experiment. This flame is of interest because it is subjected to negative stretch rates, and because only the curvature effect is present; the complications associated with strain are absent. The measured values of Ma for the IPF are significantly larger than previous measurements reported for the OPF case.

2. Computed Markstein numbers also were obtained using the RUN-1DL code and complex chemistry. Results agreed with the experiment. Computed values of *Ma* for the IPF were significantly larger than computed for the OPF case, in agreement with the measurements.

3. When the thermal expansion is artificially removed from the computations, both IPF and OPF cases are subjected to curvature effects alone, and strain effects are absent; the resulting computed Markstein numbers are identical. This indicates that the Markstein numbers associated with strain and curvature

differ, which has been suggested previously in work by Poinsot et al. [7], Bradley et al. [5] and others.

4. The difference between Markstein numbers associated with [illegible] and OH [illegible] does not appear to be due to radicals and [illegible] or due to differences in the mass diffusion of the various species, based on computations for which these quantities were varied.

ACKNOWLEDGMENTS

Support for this research was provided by NASA Grant NCC3-656. The diagnostics used were also supported by National Science Foundation Grant CTS 9123834, which is monitored by Dr. Farley Fisher.

References

[1] Sun, C. J., Sung, C. J., He, L., and Law, C. K. *Combust. & Flame* 118: pp. 108–128 (1999).

[2] Kwon, S., Tseng, I.-K., and Faeth, G. M. *Combust. & Flame* 90: pp. 230–246 (1992).

[3] Tseng, L.-K., Ismail, M. A., and Faeth, G. M. *Combust. & Flame* 95: pp. 410–426 (1993).

[4] Palm-Leis, A. and Strehlow, R. A. *Combust. & Flame* 13: pp. 111–129 (1969).

[5] Bradley, D., Gaskell, P. H., and Gu, X. J. *Combust. & Flame* 104: pp. 176–198 (1996).

[6] Echekki, T. and Mungal, M. G. *Proc. Comb. Inst. 23:* pp. 455–461 (1990).

[7] Poinsot, T., Echekki, T., and Mungal, M. G. *Comb. Sci. and Tech.* 81: pp. 45–73 (1992).

[8] Durox, D., Ducruix, S., and Candel, S. *Combust. & Flame* 125: pp. 982–1000 (2001).

[9] Ibarreta, A. F. and Driscoll, J. F. *Proc. Comb. Inst. 28:* pp. 1783–1791 (2000).

[10] Baillot, F. and Bourehla, A. *Comb. Sci. and Tech.* 126: pp. 201–224 (1997).

[11] Sinibaldi, J. O., Mueller, C. J., and Driscoll, J. F. *Proc. Comb. Inst. 27:* (1998).

[12] Mueller, C. J. Measurements of a Flame-Vortex Interaction Dynamics and Chemistry. Ph.D. thesis, University of Michigan (1996).

[13] Patnaik, G. and Kailasanath, K. In *Second Joint Meeting of US Sect. of Comb. Inst.* (March 2001).

[14] Rogg, B. Reduced Kinetic Mechanisms for Applications in Combustion Systems, chap. RUN-1DL: The Cambridge Universal Laminar Flamelet Computer Code. Springer-Verlag, Berlin-Heidelberg (1993).

[15] Rogg, B. and Wang, W. RUN-1DL - The Laminar Flame and Flamelet Code. Ruhr-Universitat Bochum (1997).

[16] [illegible]

[17] Markstein, G. H. *Journal of Aeronautical Sciences* pp. 199–209 (1951).

[18] Candel, S. M. and Poinsot, T. J. *Comb. Sci. and Tech.* 70: pp. 1–22 (1990).

[19] Djavdan, E., Darabiha, N., Giovangigli, V., and Candel, S. M. *Comb. Sci. and Tech.* 76: pp. 287–309 (1991).

[20] Egolfopoulos, F. N., Zhu, D. L., and Law, C. K. *Proc. Comb. Inst. 23:* pp. 471–478 (1990).

[21] Smooke, M. D., Puri, I. K., and Seshadri, K. *Proc. Comb. Inst. 21:* pp. 1783–1792 (1998).

[22] Egolfopoulos, F. N., Cho, P., and Law, C. K. *Combust. & Flame* 76: pp. 375–392 (1989).

[23] Matalon, M. and Matkowsky, B. J. *J. Fluid Mech.* 124: pp. 239–259 (1982).

[24] Matalon, M. and Bechtold, J. K. *Combust. & Flame* 127: pp. 1906–1913 (2001).

[25] Aung, K. T., Tseng, L.-K., Ismail, M. A., and Faeth, G. M. *Combust. & Flame* 102: pp. 526–530 (1995).

[26] Taylor, S. C. Ph.D. thesis, University of Leeds (1991).

[27] Jones, W. P. and Lindstedt, R. P. *Combust. & Flame* 73: pp. 233–249 (1988).

[28] Coffee, T. P., Kotlar, A. J., and Miller, M. S. *Combust. & Flame* 54: pp. 155–169 (1983).

Figure 1: **Experimental flame contours** of an inwardly propagating flame (IPF) at microgravity conditions are plotted for several times; time step is 4 ms. The boundary is first determined using a shadowgraph technique and then fitted with polynomials. The flame speed is calculated locally using consecutive surfaces, ΔX_n, and the time difference, Δt. Only 1 of every 2 surfaces obtained is shown for clarity.

Figure 2: **Experimental Results (Propane - $\Phi = 0.54$):** Compilation scatter plot of non-dimensional flame speed (S_u/S_u^o) versus non-dimensional curvature (δ_D^o/R_c). The size of the circles indicate the number of points averaged at that curvature location. The error bars extend one standard deviation above and below the mean for the points averaged. The slope of the least-squares fit line through point (0,1) is equal to $-Ma$, as shown in Eq. 4.

Figure 3: **Numerical Results (Propane - $\Phi = 0.6$):** Computed (S_u^o/S_u) versus non-dimensional stretch rate (Ka) for OPFs (□) and IPFs (△). The Markstein number is defined as the slope of the best linear fit (shown as a solid line) from Eq. 1. Notice that the IPF Markstein number is much larger, such that the slopes clearly do not match.

Figure 4: **Propane-Air Results:** Compilation plot showing numerical and experimental results obtained for both IPF (solid symbols) and OPF (open symbols) flames. Experimental microgravity results of current study are shown (♦). Current numerical results for IPFs and OPFs are shown as triangles (△ and ▲). This set of data is compared to numerical data obtained for IPF and OPF flames of Sun et al. [1], shown as circles (○ and ●). Note that their OPF data were modified by using our definition of burning velocity. Other experimental results for OPFs of Tseng at al. [3], Taylor [26] and Palm-Leis et al. [4] are also shown for comparison (◊). All available data show a definite difference between the Markstein values associated with OPFs and IPFs.

Figure 5: **Propane-Air IPF Case ($\Phi = 0.6$):** Computed temperature and molar concentrations of choice species across the outwardly propagating flame. The reference unstretched case is shown as the dotted lines. The solid lines represent the flame structure for the stretched case ($K = -704s^{-1}$). The $x = 0$ location corresponds to the point of maximum heat release. The origin is located to the left of the plot. Notice that stretch causes a moderate increase in final temperature and intermediate species such as H, OH and CO; this increase is linked to a large increase in burning velocity (because of the positive Ma). The increase in intermediate species is also associated with an increase in heat release. For the stretched case there is also a very noticeable increased concentration of H_2 ahead of the flame. The flame thickness, as defined from the temperature profile, is greatly diminished for the stretched flame.

Figure 6: **Propane-Air OPF Case ($\Phi = 0.6$):** Computed temperature and molar concentrations of choice species across the outwardly propagating flame. The reference unstretched case is shown as the dotted lines. The solid lines represent the flame structure for the stretched case ($K = +113s^{-1}$). The $x = 0$ location corresponds to the point of maximum heat release. The origin is now located to the right of the plot. Notice that stretch causes a small decrease in final temperature and intermediate species; this decrease is linked to a decrease in burning velocity (because of the positive Ma). The decrease in intermediate species is also associated with an decrease in heat release.

Figure 7: **Methane-Air Results:** Compilation plot showing numerical results obtained for both IPF (solid symbols) and OPF (open symbols) flames. Numerical results for complex chemistry IPFs and OPFs are shown as triangles ($\triangle$ and $\blacktriangle$). Results obtained for simple step chemistry are shown as diamonds ($\Diamond$ and $\blacklozenge$). Note that IPF Markstein values are larger then OPF values. Experimental OPF data of Tseng et al. [3, 25] are shown for comparison ($\circ$).

Figure 8: **Lewis number dependence for simple chemistry (Methane-air; $\Phi = 0.66$):** Numerical results of Markstein numbers versus Lewis number of the fuel for methane/air flames using simple one-step chemistry. Both plots show results for IPFs ($\blacklozenge$) and OPFs ($\Diamond$). Figure **8(a)** shows the dependence of Markstein number on the fuel Lewis number for the simple mechanism. Notice there is still a large discrepancy between values obtained for IPFs and OPFs. Figure **8(b)** shows results when heat release is lowered to negligible values. In this case, both flame configurations are purely curved. Both Markstein values collapse onto each other for a wide range of Lewis numbers.

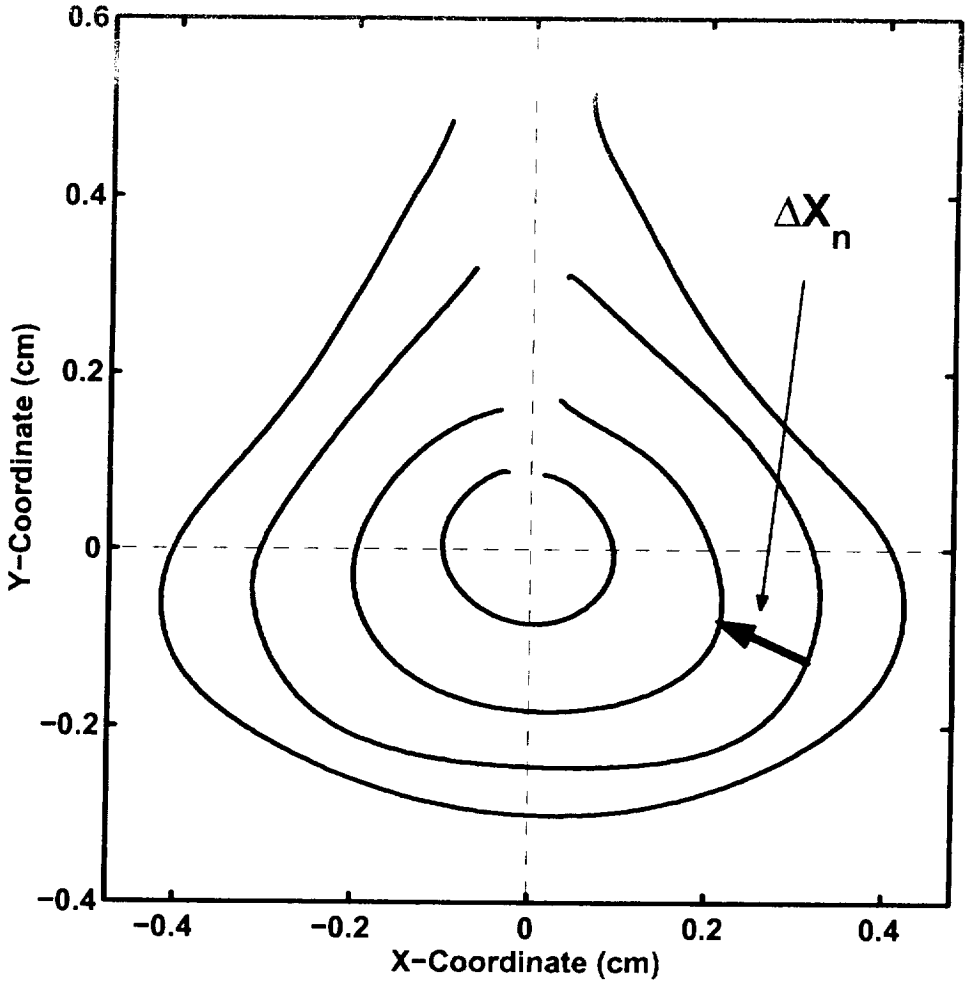

Figure 1: **Experimental flame contours** of an inwardly propagating flame (IPF) at microgravity conditions are plotted for several times; time step is 4 ms. The boundary is first determined using a shadowgraph system and then fitted with polynomials. The flame speed is calculated locally using the normal distance between surfaces, ΔX_n, and the time difference, Δt. Only 1 of every 2 surfaces obtained is shown for clarity.

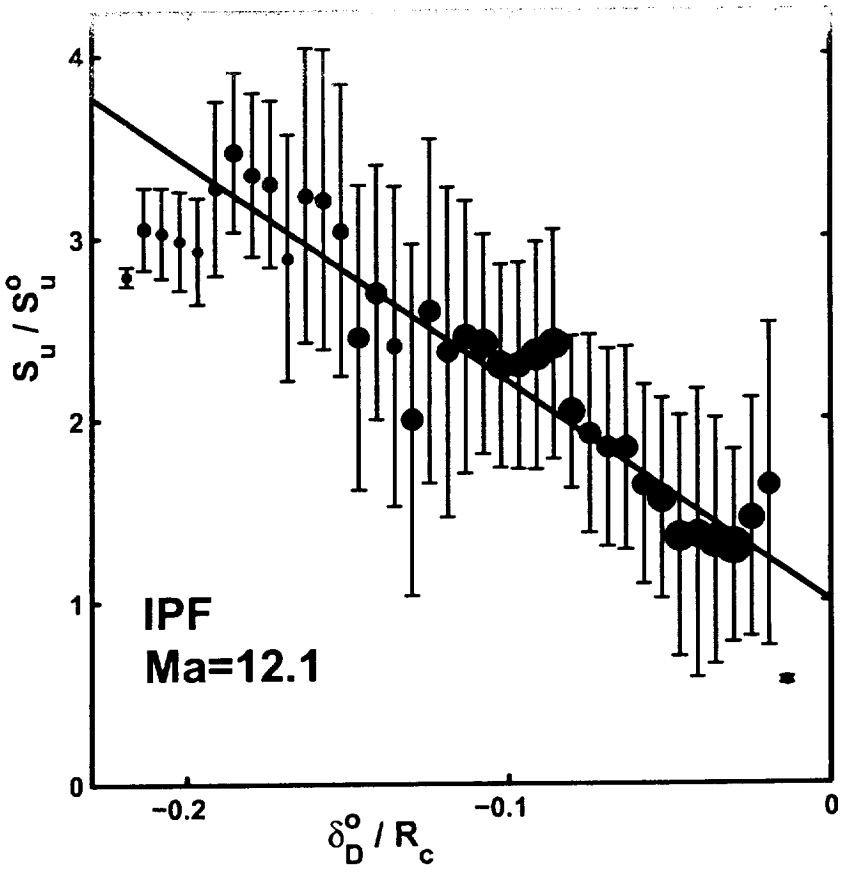

Figure 2: **Experimental Results (Propane - Φ = 0.54):** Compilation scatter plot of non-dimensional flame speed (S_u/S_u^o) versus non-dimensional curvature (δ_D^o/R_c). The size of the circles indicate the number of points averaged at that curvature location. The error bars extend one standard deviation above and below the mean for the points averaged. The slope of the least-squares fit line through point (0,1) is equal to $-Ma$, as shown in Eq. 4.

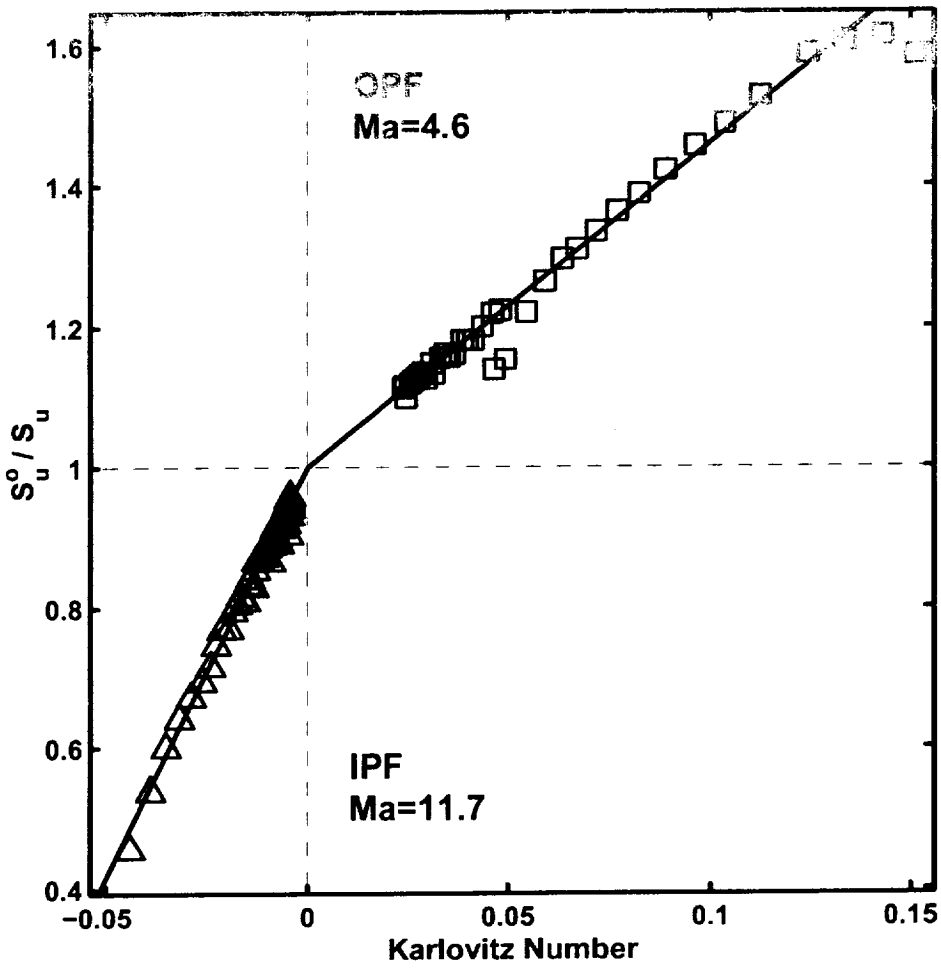

Figure 3: **Numerical Results (Propane - $\Phi = 0.6$):** Computed (S_u^o/S_u) versus non-dimensional stretch rate (Ka) for OPFs (□) and IPFs (△). The Markstein number is defined as the slope of the best linear fit (shown as a solid line) from Eq. 1. Notice that the IPF Markstein number is much larger, such that the slopes clearly do not match.

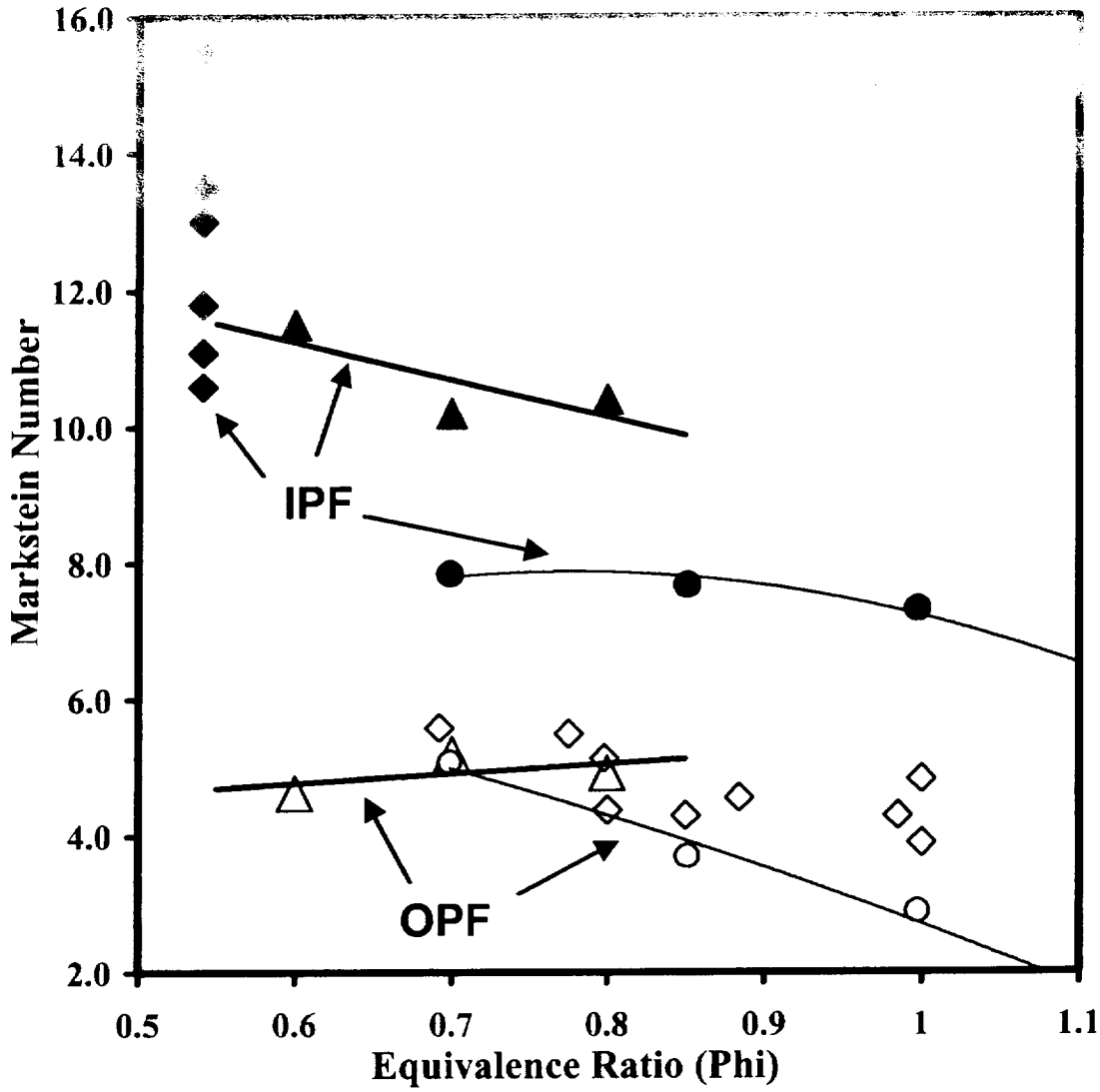

Figure 4: **Propane-Air Results:** Compilation plot showing numerical and experimental results obtained for both IPF (solid symbols) and OPF (open symbols) flames. Experimental microgravity results of current study are shown (♦). Current numerical results for IPFs and OPFs are shown as triangles (△ and ▲). This set of data is compared to numerical data obtained for IPF and OPF flames of Sun et al. [1], shown as circles (○ and ●). Note that their OPF data were modified by using our definition of burning velocity. Other experimental results for OPFs of Tseng at al. [3], Taylor [26] and Palm-Leis et al. [4] are also shown for comparison (◇). All available data show a definite difference between the Markstein values associated with OPFs and IPFs.

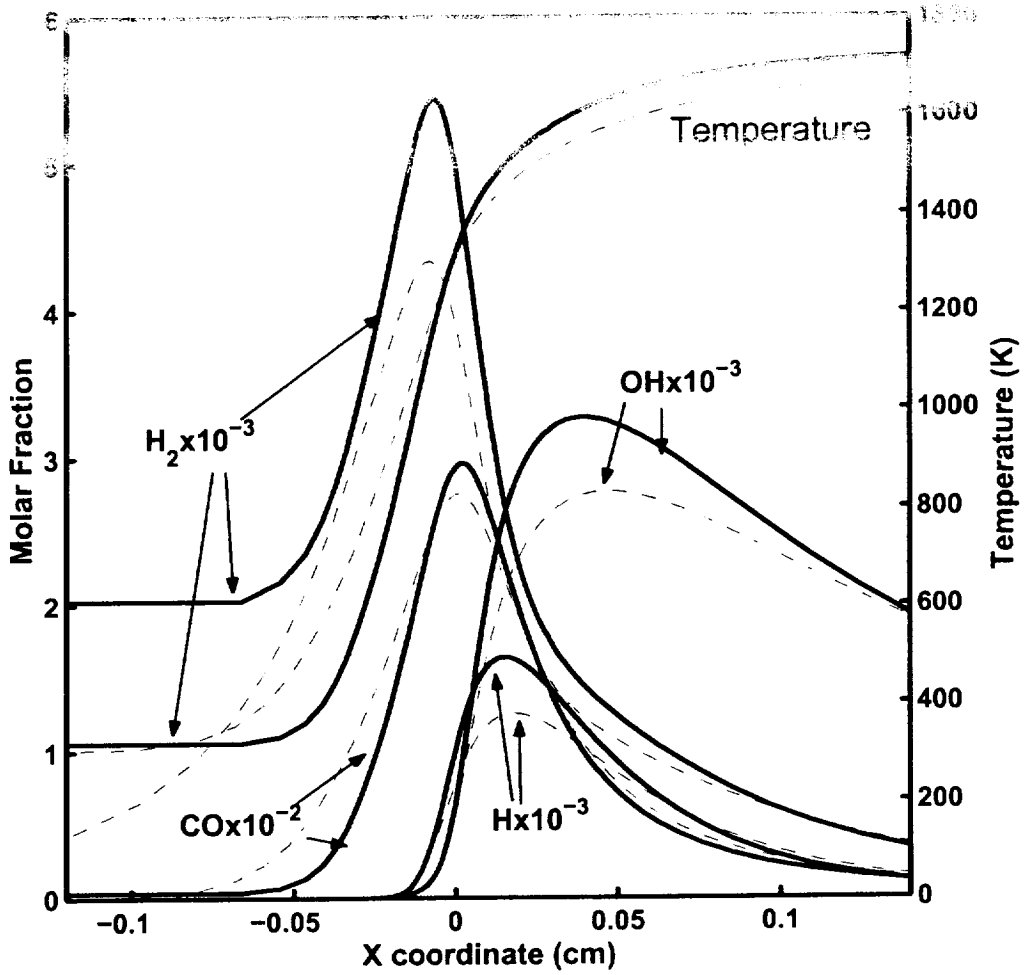

Figure 5: **Propane-Air IPF Case ($\Phi = 0.6$):** Computed temperature and molar concentrations of choice species across the outwardly propagating flame. The reference unstretched case is shown as the dotted lines. The solid lines represent the flame structure for the stretched case ($K = -704s^{-1}$). The $x = 0$ location corresponds to the point of maximum heat release. The origin is located to the left of the plot. Notice that stretch causes a moderate increase in final temperature and intermediate species such as H, OH and CO; this increase is linked to a large increase in burning velocity (because of the positive Ma). The increase in intermediate species is also associated with an increase in heat release. For the stretched case there is also a very noticeable increased concentration of H_2 ahead of the flame. The flame thickness, as defined from the temperature profile, is greatly diminished for the stretched flame.

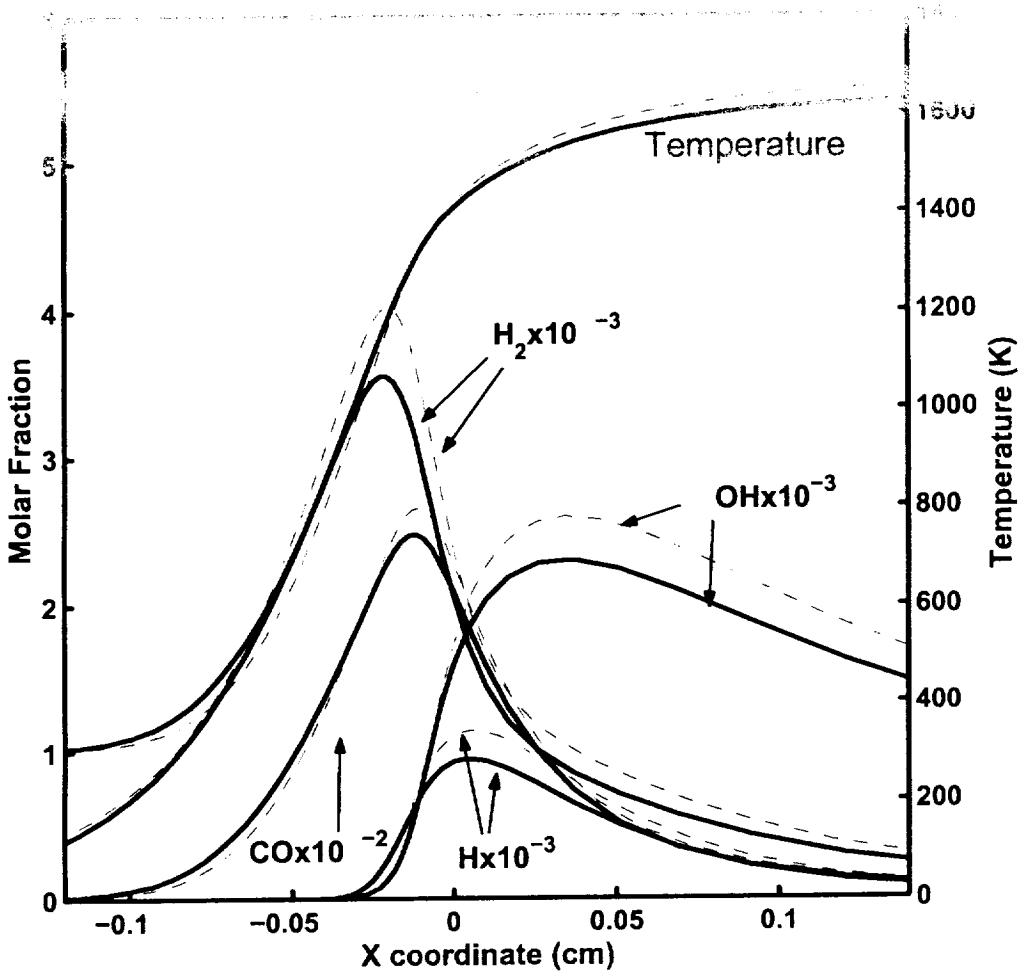

Figure 6: **Propane-Air OPF Case ($\Phi = 0.6$):** Computed temperature and molar concentrations of choice species across the outwardly propagating flame. The reference unstretched case is shown as the dotted lines. The solid lines represent the flame structure for the stretched case ($K = +113s^{-1}$). The $x = 0$ location corresponds to the point of maximum heat release. The origin is now located to the right of the plot. Notice that stretch causes a small decrease in final temperature and intermediate species; this decrease is linked to a decrease in burning velocity (because of the positive Ma). The decrease in intermediate species is also associated with an decrease in heat release.

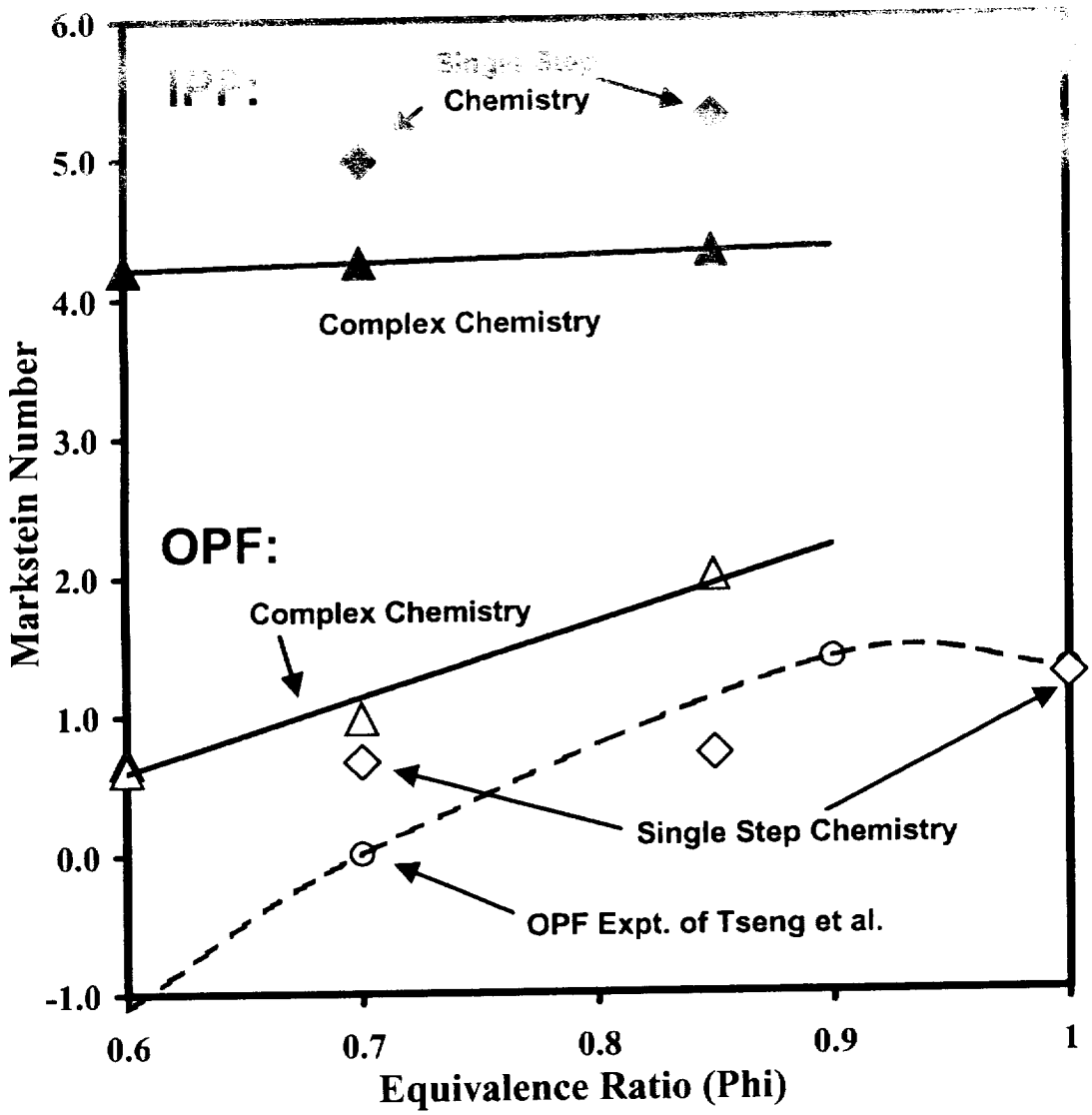

Figure 7: **Methane-Air Results:** Compilation plot showing numerical results obtained for both IPF (solid symbols) and OPF (open symbols) flames. Numerical results for complex chemistry IPFs and OPFs are shown as triangles (△ and ▲). Results obtained for simple step chemistry are shown as diamonds (◊ and ♦). Note that IPF Markstein values are larger then OPF values. Experimental OPF data of Tseng et al. [3, 25] are shown for comparison (○).

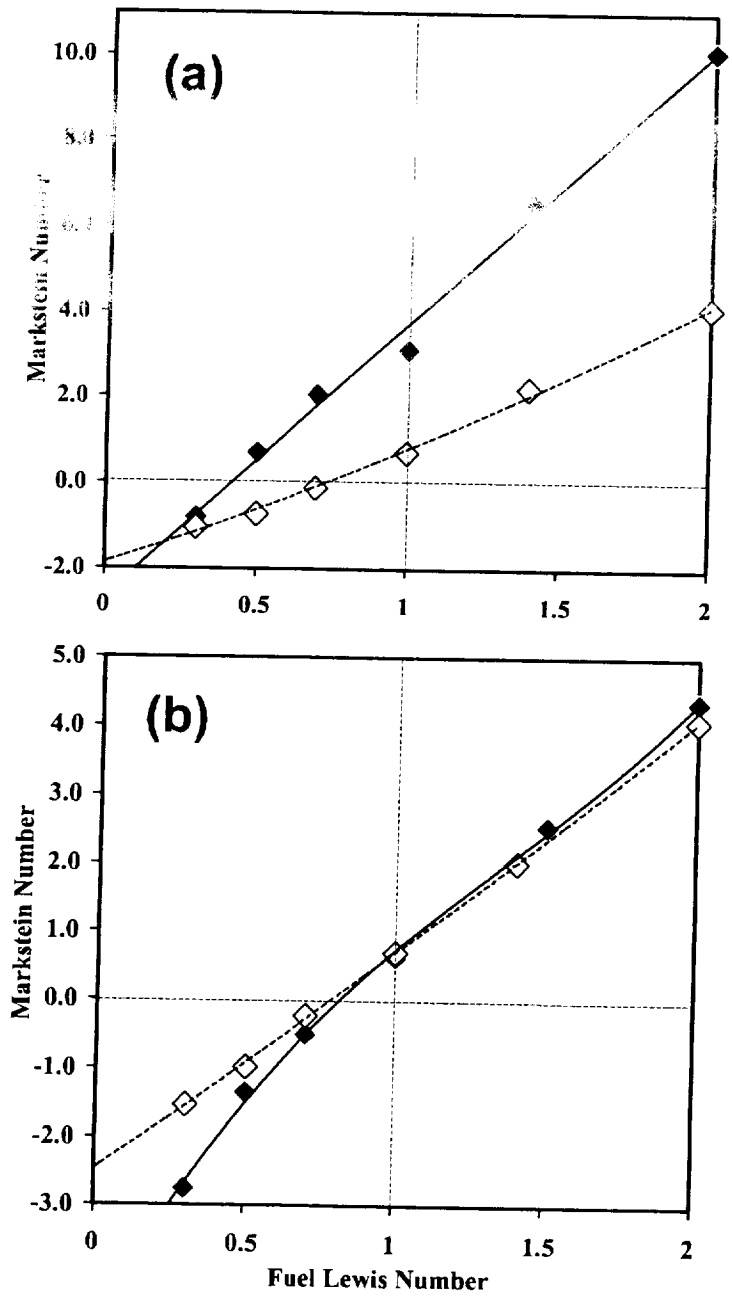

Figure 8: **Lewis number dependence for simple chemistry (Methane-air; $\Phi = 0.66$):** Numerical results of Markstein numbers versus Lewis number of the fuel for methane/air flames using simple one-step chemistry. Both plots show results for IPFs (♦) and OPFs (◊). Figure **8(a)** shows the dependence of Markstein number on the fuel Lewis number for the simple mechanism. Notice there is still a large discrepancy between values obtained for IPFs and OPFs. Figure **8(b)** shows results when heat release is lowered to negligible values. In this case, both flame configurations are purely curved. Both Markstein values collapse onto each other for a wide range of Lewis numbers.